JOC The Journal of Organic Chemistry

Article

pubs.acs.org/joc

Ketyl Radical Formation via Proton-Coupled Electron Transfer in an Aqueous Solution versus Hydrogen Atom Transfer in Isopropanol after Photoexcitation of Aromatic Carbonyl Compounds

Xiting Zhang,[†] Jiani Ma,[*,‡] Songbo Li,[†] Ming-De Li,[†] Xiangguo Guan,[†] Xin Lan,[†] Ruixue Zhu,[†] and David Lee Phillips[*,†]

[†]Department of Chemistry, The University of Hong Kong, Pokfulam Road, Hong Kong, P. R. China

[‡]Key Laboratory of Synthetic and Natural Functional Molecule Chemistry of Ministry of Education, College of Chemistry and Materials Science, Northwest University, Xi'an 710127, P. R. China

Supporting Information

ABSTRACT: The excited $n\pi^*$ and $\pi\pi^*$ triplets of two benzophenone (BP) and two anthraquinone (AQ) derivatives have been observed in acetonitrile, isopropanol, and mixed aqueous solutions using time-resolved resonance Raman spectroscopic and nanosecond transient absorption experiments. These experimental results, combined with results from density functional theory calculations, reveal the effects of solvent and substituents on the properties, relative energies, and chemical reactivities of the $n\pi^*$ and $\pi\pi^*$ triplets. The triplet $n\pi^*$ configuration was found to act as the reactive species for a subsequent hydrogen atom transfer reaction to produce a ketyl radical intermediate in the isopropanol solvent, while the triplet $\pi\pi^*$ undergoes a proton-coupled electron transfer (PCET) in aqueous solutions to produce a ketyl radical intermediate. This PCET reaction, which occurs via a concerted proton transfer (to the excited carbonyl group) and electron transfer (to the excited phenyl ring), can account for the experimental observation by several different research groups over the past 40 years of the formation of ketyl radicals after photolysis of a number of BP and AQ derivatives in aqueous solutions, although water is considered to be a relatively "inert" hydrogen-donor solvent.

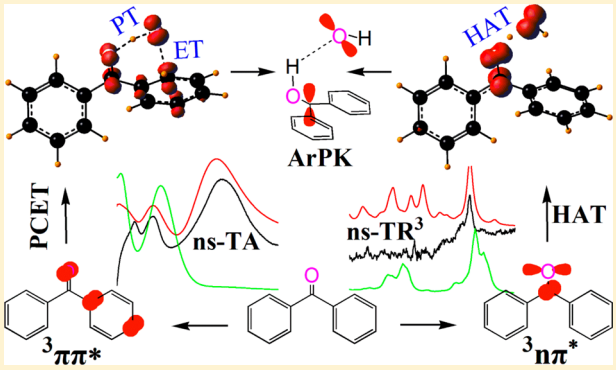

INTRODUCTION

Benzophenone (BP) derivatives such as ketoprofen, fenofibrate, fenofibric acid, and others can be used as nonsteroidal anti-inflammatory drugs (NSAIDs) to treat musculoskeletal and joint disorders, osteoarthritis, rheumatoid arthritis, and other inflammatory conditions.[1] BP and its derivatives are also important chromophores that, after absorption of a photon of light, may give rise to a wide range of reactions in biological systems such as electron transfer, hydrogen abstraction, triplet−triplet energy transfer, and photosensitization reactions that in some cases can cause damage to DNA and/or other biological molecules.[2] The photochemistry of anthraquinone (AQ) derivatives in aqueous solutions has also received increasing interest as a platform for developing photoremovable protecting groups.[3]

Several groups over the past several decades have reported observing the formation of an arylphenyl ketyl radical species (ArPK) after ultraviolet photoexcitation of BP and some of its derivatives in aqueous solutions, although water is considered to be a relatively "inert" hydrogen-donor solvent.[4] The time-resolved resonance Raman spectrum (ns-TR^3) of the ArPK intermediate observed in a neutral aqueous solution appears to be essentially identical to that detected in an isopropanol (IPA) solution,[5] in which a traditional photoreduction reaction via hydrogen atom transfer (HAT) takes place. However, it is acknowledged that an analogous HAT from water may not be easy because this would be a very endergonic process (about ΔG = 85 kJ/mol and ΔH = 28 kJ/mol for BP),[6] which suggests there may be a possible change in the photoreduction mechanism for aromatic carbonyls from HAT pathway solvents such as IPA to some other pathways in aqueous solutions. Knoll and co-workers[4c] and Leigh and co-workers[4a] reported flash photolysis experiments aimed at better understanding the formation mechanism of ArPK from the triplet state of BP in pure water and basic aqueous solutions. They concluded that the ArPK radicals were formed in a combined electron and proton transfer step, and further support for this view was recently provided by results from ns-TR^3 spectroscopy experiments on BP and several of its derivatives.[4h] However, there are still some questions that remain to be addressed. First, a clear and definitive electronic characterization ($n\pi^*$ or $\pi\pi^*$)

Received: March 23, 2016
Published: June 6, 2016

DOI: 10.1021/acs.joc.6b00620
J. Org. Chem. 2016, 81, 5330−5336

of the BP molecule and its counterpart AQ that reacts and leads to formation of the ArPK intermediate in aqueous solutions is still needed. The aromatic carbonyls' lowest excited triplet state is decisive for the reactivity of the carbonyl compound, which may be altered either by substitution or by solvent effects.[7] However, it is not yet clear if one or both of the $n\pi^*$ and $\pi\pi^*$ triplet states reacts to produce the ArPK species in aqueous media. Second, the formation mechanism of an ArPK radical in an aqueous solution is still uncertain. The $n\pi^*$ triplet, not the $\pi\pi^*$ triplet, is generally accepted as the reactive species for a HAT from aliphatic or benzylic hydrogen donor systems. In an aqueous solution, which triplet ($n\pi^*$ or $\pi\pi^*$) is responsible for the ArPK formation according to either a HAT or a proton-coupled electron transfer (PCET) process? Chen and co-workers recently performed CASSCF calculations for 3-(hydroxymethyl)benzophenone and 2-(1-hydroxyethyl)-9,10-anthraquinone in water and proposed that the $\pi\pi^*$ triplet is the key species associated with subsequent excited state intramolecular proton transfer reactions,[8] while similar CASSCF calculations on valerophenone in water indicated that the $n\pi^*$ triplet is the key species in a subsequent excited state 1,5-H-shift transfer reaction.[9] This suggests the need to explore both possibilities in a theoretical study on the formation mechanism of an ArPK radical intermediate from the triplet states of BPs and AQs in aqueous solutions.

The above questions motivated us to conduct a mechanistic study on the triplet reactivity of BP (**1**), 4-phenylbenzophenone (**2**), 2-(1-hydroxyethyl)-9,10-anthraquinone (**3**), and 2-(p-hydroxymethyl)-phenylanthraquinone (**4**) (Scheme 1) in IPA and neutral mixed aqueous solutions (1/1 ACN/H_2O) using nanosecond transient absorption (ns-TA) and ns-TR^3 experiments. This set of compounds was chosen to elucidate how the aromatic carbonyls' lowest excited triplet states and reaction mechanisms are altered by substitution and solvent effects and also which triplet state reacts to form the ArPK intermediate observed in neutral aqueous solutions. In addition, density functional theory (DFT) calculations with the hybrid M062X functional at the 6-311+G(d, p) level of theory were performed to examine the structures and properties of possible triplet state intermediates and their reaction pathways in IPA and a neutral aqueous solution. The M06-2X functional was chosen because it was found to give excellent performance for the hydrogen-transfer barrier height calculations, proton affinities of conjugated systems, hydrogen bonding, electronic excitation, thermochemistry, kinetics, and noncovalent interactions for a number of main-group compounds.[10] A comparison of these time-resolved experimental results with those from the DFT calculations elucidates how the aromatic carbonyls' lowest excited triplet state and reaction mechanism are altered by substitution and solvent effects and also which triplet state reacts to form the ArPK intermediate observed in neutral aqueous solutions.

Scheme 1. Structural Formula of the Compounds Studied

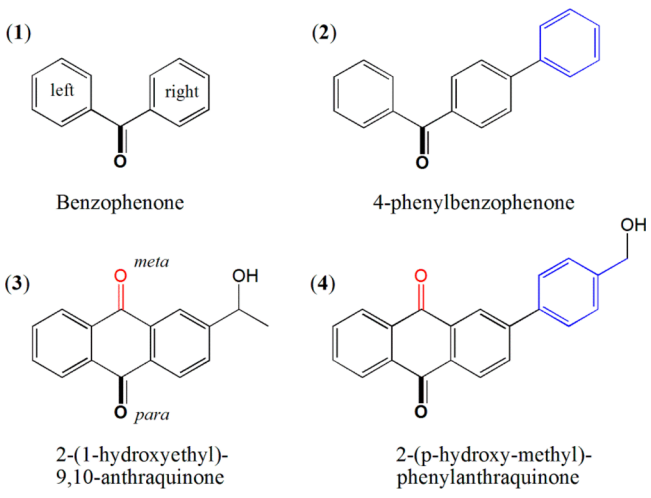

RESULTS AND DISCUSSION

Figure 1 depicts the visualized spin density populations of the $n\pi^*$ and $\pi\pi^*$ species for compounds **1**, **2**, **3** and **4**. For $(\mathbf{1})^3n\pi^*$ and $(\mathbf{2})^3n\pi^*$, two radicals mainly localize on the C p_y and the O p_x orbital of the carbonyl group, resulting in some single C−O bonds with a radical O atom character. No appreciable spin distributed to two phenyl rings. However, two radicals are positioned parallel on the carbonyl O p_y orbital: the C p_y orbital adjacent to the carbonyl and the *para* C p_y orbital of the right phenyl ring for $(\mathbf{1})^3\pi\pi^*$ and $(\mathbf{2})^3\pi\pi^*$. The spin delocalized character of the $\pi\pi^*$ species apparently reduces the radical character of the carbonyl O atom while generating some double C−O bond character. No appreciable spin resides on the left phenyl ring. The AQs (**3** and **4**) have more $n\pi^*$ and $\pi\pi^*$ species than the BPs due to the existence of two carbonyl groups. Each $n\pi^*$ or $\pi\pi^*$ species of the AQs exhibits a spin character similar to those of the BPs. The $n\pi^*/\pi\pi^*$ electronic properties of the BPs and AQs of interest here reveal the clear and definitive difference that the photoexcitation invokes only one carbonyl group in the $n\pi^*$ state, while one carbonyl group and one phenyl group are photoexcited in the $\pi\pi^*$ state, which is consistent with CASSCF results.[9]

This naturally brings up the question of whether the ArPK formation would depend differently on the $n\pi^*$ and $\pi\pi^*$ species. To answer this question, it is important to evaluate the relative stability of the above triplet species for each compound (Figure 2). The free energy gaps ΔG of ACN for **1** (5.6 kcal/mol, $n\pi^*$ triplet) and **2** (−2.7 kcal/mol, $\pi\pi^*$ triplet) agree well with experimental observations.[7,11] The ΔG of ACN for **3** and **4** reveals some interesting information. The relative position between the excited carbonyl and substituent group (Scheme 1 and Figures 1 and 2) has little influence on the $n\pi^*$ species, as the ΔG values between $(\mathbf{3})^3n\pi^*p$ and $(\mathbf{3})^3n\pi^*m$ and between $(\mathbf{4})^3n\pi^*m$ and $(\mathbf{4})^3n\pi^*p$) are small; however, it exerts a significant effect on the $\pi\pi^*$ species as indicated by the noticeably larger ΔG between $(\mathbf{3})^3\pi\pi^*m$ and $(\mathbf{3})^3\pi\pi^*p$ (6.8 kcal/mol) and also between $(\mathbf{4})^3\pi\pi^*m$ and $(\mathbf{4})^3\pi\pi^*p$ (12.3 kcal/mol). Integration of the spin population characters in Figure 1 and the energy results in Figure 2 for the BPs and AQs reveal that some radicals may locate on the *para* C p_y orbital of the excited phenyl ring rather than on the relative *meta* position between the excited carbonyl and the substituent group so that the relative *para* position facilitates the spin delocalization more efficiently to stabilize the $\pi\pi^*$ species and even changes the order of the lowest excited triplet ($n\pi^*$, $\pi\pi^*$). $(\mathbf{3})^3\pi\pi^*m'$ and $(\mathbf{4})^3\pi\pi^*m'$ have energies 1.8 and 9.0 kcal/mol higher than those of $(\mathbf{3})^3\pi\pi^*p$ and $(\mathbf{4})^3\pi\pi^*p$, respectively, which reveals that the electron-donating group on the excited phenyl ring would stabilize the $\pi\pi^*$ species. In addition, the spin delocalized to the phenyl ring leads to the larger dipole moment (Table 1S) so that the $^3\pi\pi^*$ species can be more stabilized than the $^3n\pi^*$ species with an increase in the solvent polarity (Figure 2).[7]

DOI: 10.1021/acs.joc.6b00620
J. Org. Chem. 2016, 81, 5330−5336

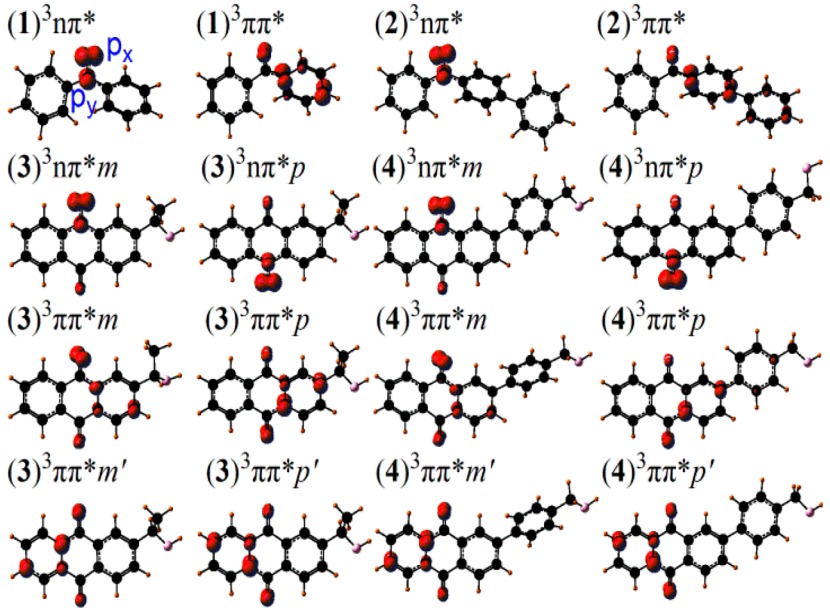

Figure 1. Visualized spin density (isovalue = 0.02) plots for the possible $n\pi^*$ and $\pi\pi^*$ species of compounds **1**, **2**, **3**, and **4** calculated at the uM062X/6-311+G(d, p) level of theory. The superscript 3 stands for the triplet state; the italic *m* and *p* stand for the spin populated mainly on the *meta* and *para* carbonyl groups, respectively, relative to the substituent group, and the apostrophe stands for the phenyl ring without the substituent group.

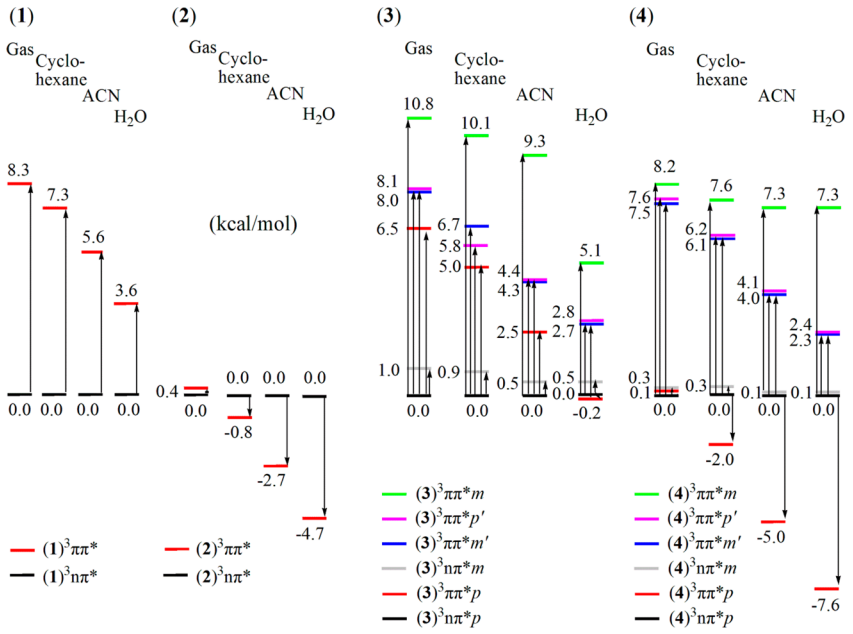

Figure 2. Relative free energies (kcal/mol) for the possible $n\pi^*$ and $\pi\pi^*$ species of compounds **1**, **2**, **3**, and **4** calculated at the uM062X/6-311+G(d, p) level of theory in gas and uM062X/6-311++G(d, p)//uM062X/6-311+G(d, p) level of theory in cyclohexane, ACN, and H_2O.

We note that using the M062X DFT method provides the opportunity to simulate both the UV−vis and Raman spectra for the exited triplet $n\pi^*$ and $\pi\pi^*$ of aromatic carbonyls, which can be used to make assignments of the experimental TA and TR^3 spectra in ACN for **1**, **2**, **3**, and **4** because it is well-accepted that BP and AQ compounds undergo mainly photophysical processes in the inert organic solvent ACN and no appreciable photochemical reaction takes place. From the ns-TA results (Figure 3I), significant absorbance appears at 323 and 525 nm for **1**. The calculated UV−vis spectrum of $(\mathbf{1})^3n\pi^*$ exhibits a spectral profile similar to that in the experimental results. Inspection of Figure 4I shows that the vibrational frequency patterns in the ns-TR^3 of **1** can be found in the calculated Raman spectrum of $(\mathbf{1})^3n\pi^*$ (although the intensities are different because the experimental spectra are resonantly enhanced, while the calculated ones are not). Compound **2** exhibits a significantly different ns-TA spectrum in ACN compared to that of **1**. The absorption bands at 374, 418, 455, and 510 nm appear to coincide with the spectral pattern calculated from TD-M062X for the $(\mathbf{2})^3\pi\pi^*$species (Figure 3II). The ns-TR^3 (Figure 4II) for **2** also supports the $(\mathbf{2})^3\pi\pi^*$species with the bands of 1480, 1518, 1578, and 1591 cm^{-1}. The AQ compound **3** exhibited distinctly different ns-TA and ns-TR^3 spectra from the BPs. One band at 381 nm and two shoulder features around 456 and 600 nm can be found (Figure 3III). The TD-M062X calculations for $(\mathbf{3})^3n\pi^*m$ have a

DOI: 10.1021/acs.joc.6b00620
J. Org. Chem. 2016, 81, 5330−5336

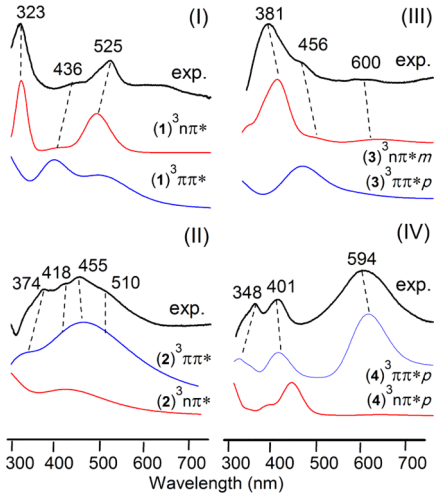

Figure 3. Comparison of the experimental ns-TA spectra in ACN and the calculated UV−vis spectra of the *nπ** and *ππ** species at the uM062X/6-311+G(d, p) level of theory.The black dashed line shows the correlation of the experimental spectra to the calculated spectra.

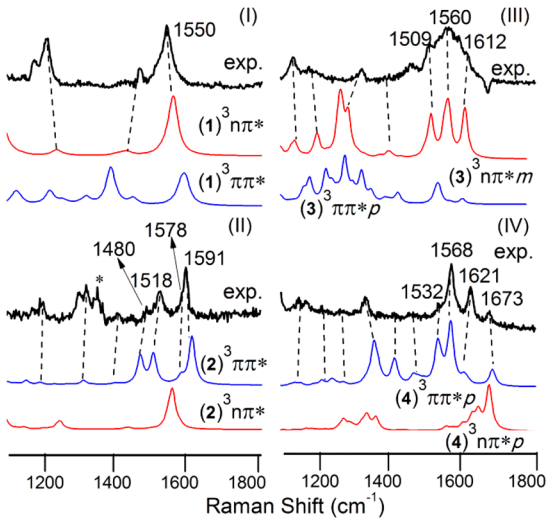

Figure 4. Comparison of the experimental ns-TR^3 spectra in ACN and the calculated UV−vis spectra of the *nπ** and *ππ** species at the uM062X/6-311+G(d, p) level of theory. The black dashed line is connected to the experimental spectra and paired calculated spectra. The asterisks mark regions affected by solvent subtraction artifacts and/or stray light.

spectral profile analogous with that of the ns-TA spectra. The comparison between the ns-TR^3 spectra with characteristic bands of 1507, 1564, and 1613 cm^{-1} and the calculated Raman spectrum of (**3**)^3*nπ*m* suggests that this is the species present in ACN (Figure 4III). The ns-TA of **4** was very different from that of **3** (Figure 3IV). The three predicted bands at 308, 410, and 605 nm for (**4**)^3*ππ*p* are in good agreement with the ns-TA spectra showing bands at 348, 401, and 594 nm. Furthermore, the Raman bands observed in the ns-TR^3 (1532, 1568, 1621, and 1673 cm^{-1}) spectra correlate with the calculated Raman bands for (**4**)^3*ππ*p* and provide further support for (**4**)^3*ππ*p* being the main species present after photoexcitation of **4** (Figure 4IV). The consistent correlation between the ns-TA/ns-TR^3 experimental results and the calculated UV−vis/Raman results, along with relative energetics deduced from the free energy calculations, indicates that the M062X method is reasonably reliable to predict the *nπ** and *ππ** configurations of the excited triplets for the aromatic carbonyl compounds of interest. It is more efficient to perform an M062X structural optimization and analytic frequency calculation to provide vibrational spectra for the triplet *nπ** and *ππ** aromatic carbonyl compounds than to use the much more computational resource-demanding CASSCF method.

The generation of the ArPK species of **1** and **2** in IPA and ACN-H_2O was investigated next. The H atom of the 2° C−H bond in IPA and the O−H bond in IPA and H_2O are possible hydrogen donors (Scheme 2). Figure 5 depicts the visualized

Scheme 2. Diagram of the Different Pathways of the Photoreduction Reaction

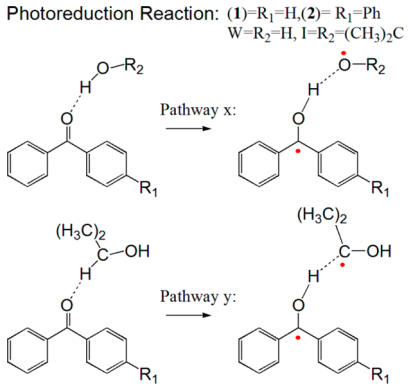

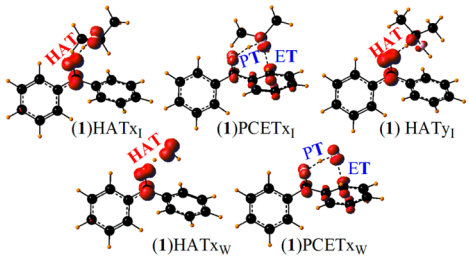

Figure 5. Visualized spin density (isovalue = 0.02) plots for the possible HAT and PCET transition states of compound **1** calculated at the uM062X/6-311+G(d, p) level of theory. The subscripts I and W mean IPA and water, respectively. The letters x and y mean H atom transfer from the O−H bond and the 2° C−H bond from IPA, respectively.

spin density populations of the possible transition states (TSs) for compound **1** located by the M062X method, and it can be seen that these TSs exhibit quite different HAT and PCET properties. It is suggested that for (**1**)HATx_I, (**1**)HATy$_I$, and (**1**)HATy$_w$, the unpaired spin density shifts from the carbonyl O atom to the 2° C−H bond of (**1**)HATy$_I$ or the O−H bond of (**1**)HATx$_I$ and (**1**)HATy$_w$ as the proton transfers (PT), and the HAT region (Figure 5) is predominately accounted for by atomic orbitals oriented along the hydrogen donor−acceptor axis with a *σ*-bonding interaction. In contrast, for the PT for (**1**) PCETx$_I$ and (**1**) PCETx$_w$, the unpaired spin density shifts from the phenyl *ortho* C atom (not the carbonyl O atom) to the O−H bond of (**1**) PCETx$_I$ and (**1**) PCETx$_w$. The PT interface (Figure 4) is predominately accounted for by the 2p orbitals perpendicular to the proton donor−acceptor axis with a *π*-bonding interaction, while the electron transfer (ET) region is predominately accounted for by the atomic orbitals oriented along the electron donor−acceptor axis with a *σ*-bonding

DOI: 10.1021/acs.joc.6b00620
J. Org. Chem. 2016, 81, 5330−5336

interaction. The TSs for the PCET have a spin delocalized character more significant than that of the TSs for the HAT. There exists some spin distributed on the phenyl rings for the PCET but not for the HAT. Examination of Figure 5 clearly illustrates that the TSs for the PCET pathways exhibit triplet $\pi\pi^*$ character, while the TSs for the HAT pathways have triplet $n\pi^*$ character (Figure 1). The radical delocalization may facilitate the stability of the PCET compared to that of the HAT. Recently, Hammes-Schiffer and co-workers calculated TS structures for the HAT and PCET for the phenoxyl using phenol as the hydrogen donor at the DFT/M06-2X/6-311+G** level of theory and found that the π-electron in phenol facilitates the electron coupling in the TS of PCET.[12] The TS of PCET also can be located using phenol as the hydrogen donor for 4-methoxybenzophenone (Figure 1S). However, it should be noted that only the TS of HAT ($HATy_I$), not the TS of PCET, was located for the BP using the IPA 2° C−H bond as the hydrogen donor. The absence of lone-paired electrons or π-electrons on the 2° C−H bond of IPA resulted in the lack of the TS of a PCET. The possible TSs for compound **2** in IPA and ACN-H_2O were also located and exhibited spin-density characters very similar to those found for compound **1** in IPA and ACN-H_2O (Figure 2S).

The intrinsic reaction coordinate (IRC) calculations (Figure 3S) indicate that all of the TSs for HAT and PCET located for **1** and **2** in IPA and ACN-H_2O, respectively, connect to the triplet $n\pi^*$ and $\pi\pi^*$ species. On the other hand, all of the TSs of HAT go forward to the ArPK species. The visualized spin density populations of the ArPK species for **1** and **2** in IPA and H_2O (Figure S4) clearly reveal that one radical is localized on the carbonyl C atom and the other radical resides on the solvent molecule.

There exists three pathways of **1** in IPA toward the formation of the ArPK species as depicted in Figure 6A, and the preferred pathway starts from the $n\pi^*$ species $(\mathbf{1})^3n\pi^*x_I$ and $(\mathbf{1})^3n\pi^*y_I$ via a HAT TS, $(\mathbf{1})HATy_I$, with an activation energy of 5.3 kcal/mol followed by the formation of an ArPK species, $(\mathbf{1})ArPKy_I$. The reaction pathways of **2** with IPA (Figure 6B) are somewhat different from **1**. It can be found that **2**, with its lowest $\pi\pi^*$ triplet state $(\mathbf{2})^3\pi\pi^*x_I$, reacts through the thermally populated $(\mathbf{2})^3n\pi^*x_I$ and $(\mathbf{2})^3n\pi^*y_I$ then goes through $(\mathbf{2})HATy_I$ with an overall reaction barrier of 8.9 kcal/mol to produce $(\mathbf{2})ArPKy_I$. This result indicates that the lowest $\pi\pi^*$ species, $(\mathbf{2})^3\pi\pi^*x_I$, is much less reactive than the lowest $n\pi^*$ state, $(\mathbf{1})^3n\pi^*x_I$, toward HAT in IPA. That is, the reactivity is basically due to $n\pi^*$ triplet states $(\mathbf{2})^3n\pi^*y_I$, while $(\mathbf{2})^3\pi\pi^*x_I$ states are essentially unreactive.[7] In addition, Figures 6A and 6B also reveal that the 2° C−H bond of IPA is a more reactive hydrogen-donor with a lower energy barrier, leading to the ArPK species with a larger exothermicity compared to that of the O−H bond of IPA.

The HAT process was generally accepted for the photoreduction of aromatic carbonyls in IPA.[5] Figures 4C and 4D reveal that the O−H bond of H_2O is a more "inert" hydrogen donor and, to form the ArPK species, requires an activation energy with BPs higher than that of the O−H and 2° C−H bonds of IPA. In addition, Figures 4C and 4D also reveal that it is an endergonic process for ArPK formation from BPs and H_2O,[6] which is significantly different from the photoreduction between BPs and IPA and may not be easy for an analogous HAT from water. However, Figures 4C and 4D indicate a change in the ArPK formation route for carbonyl compounds in ACN-H_2O. The TSs of $(\mathbf{1})PCETx_W$ and $(\mathbf{2})PCETx_W$ directly

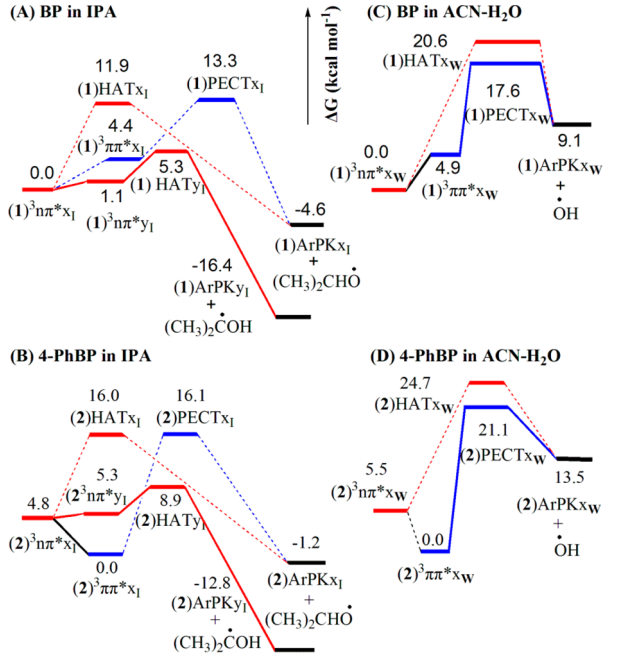

Figure 6. DFT-computed free energy surface for the formation of the ArPK species at the uM062X/6-311++G(d, p)-SMD (IPA)//uM062X/6-311+G(d, p) level of theory for A and B and at the uM062X/6-311++G(d, p)-SMD (ACN)//uM062X/6-311+G(d, p) level of theory for C and D. The subscripts I and W mean IPA and water, respectively. The letters x and y mean H atom transfer from the O−H bond and the 2° C−H bond from IPA, respectively.

connected to the $\pi\pi^*$ states are lower by 3.0 and 3.6 kcal/mol than those of $(\mathbf{1})HATx_W$ and $(\mathbf{2})HATx_W$ directly connected to the $n\pi^*$ species, respectively, which leads the photoreduction to be more feasible. Furthermore, the $\pi\pi^*$ triplet is responsible for the PCET process whether or not it is the lowest excited state. The analogous PCET from water may then be easier than the HAT from water. Compound **2** with the lowest $\pi\pi^*$ state is less reactive (energy barrier of 21.1 kcal/mol) than compound **1** with the lowest $n\pi^*$ state (17.6 kcal/mol), which is in good agreement with the experimental observations.[7] The same spin distributions (Figure 4S) for $(\mathbf{1})ArPKy_I$ generated in IPA and $(\mathbf{1})ArPKx_W$ generated in H_2O can account for the detection of a ketyl radical species of **1** and **2** in neutral aqueous solutions[4] and the analogous ns-TR[3] spectra of the ArPK intermediate observed in neutral aqueous solutions and in an IPA solution.[5] The situation for AQ compounds such as **3** and **4** is more complicated because they can undergo photoredox reactions in neutral aqueous solutions in competition with photoreduction, as experimentally observed by several research groups.[13] Analogous calculations were not done here due to this additional complexity. Further theoretical and experimental studies of the competition between and the conditions that lead to photoreduction, photohydration, and photoredox reactions of BPs and AQs in solution are planned and will be reported in due course.

CONCLUSIONS

The electronic configuration, free energy, calculated UV, and Raman spectra of both excited triplet $n\pi^*$ and $\pi\pi^*$ intermediates of selected aromatic carbonyl compounds have been presented in detail here using the M062X method. Comparison of the theoretical results for the $n\pi^*$ and $\pi\pi^*$

DOI: 10.1021/acs.joc.6b00620
J. Org. Chem. 2016, 81, 5330−5336

species provides an opportunity to make assignments for the experimental ns-TA and ns-TR^3 spectra for the compounds examined. This comparison indicates that solvent and/or substituent effects can affect the relative order of the $n\pi^*$ and $\pi\pi^*$ states. Both HAT and PCET pathways were found to be directed toward the generation of an ArPK species. Furthermore, PCET appears to be the preferred route for BPs in neutral aqueous solutions, which can account for the formation of ketyl radicals after photoexcitation of BP and some of its derivatives in aqueous solutions that has been reported by a number of research groups in the literature over the past 40 years.[4] Because much of the interest in BP, AQ, and other aromatic carbonyl compounds involves their photochemistry in biological and other aqueous environments, the present results suggest that PCET processes to form radicals may be more prevalent than previously thought, and triplet $\pi\pi^*$ states of aromatic carbonyl compounds are more reactive in water than generally assumed.

EXPERIMENTAL SECTION

Benzophenone of BP (**1**) and 4-phenylbenzophenone (**2**) are commercially available. 2-(1-Hydroxyethyl)-9,10-anthraquinone (**3**) and 2-(*p*-hydroxy-methyl)-phenylanthraquinone (**4**) were synthesized following reported literature methods.[13] Spectroscopic-grade acetonitrile (MeCN), isopropyl alcohol (IPA), and deionized water were used. All of the mixed solvent ratios are volumetric ratios.

Ns-TA Experiments. The ns-TA measurements were carried out on a commercial laser flash photolysis setup. A 266 nm pump laser pulse was obtained from the fourth harmonic output of an Nd:YAG Q-switched laser, and the probe light was provided by a 450 W xenon lamp. The sample in a 1 cm flow cell was excited by the pump laser, and the probe light from the xenon lamp was passed through the sample at a right angle to the path of the exciting pulse. After passing through the sample, the analyzing light was directed to a monochromator/spectrograph, and the transmission properties of the sample before, during, and after the exciting pulse were acquired by a charge coupled device (CCD). Unless otherwise indicated, the ns-TA experiments were carried out in air-saturated solutions, and the sample solutions were prepared to yield the same absorbance at the specified λ_{exc} so that the same number of photons was absorbed for the same irradiating conditions in each case. All sample solutions were prepared with an absorbance of 1 at 266 nm.

Ns-TR^3 Experiments. The ns-TR^3 experiments were performed using an experimental apparatus and methods described previously,[4e−h] and only a brief description is given here. The 266 nm pump wavelength and probe wavelengths of 319.9 nm (used for **1** and **2**), 368.9 nm (used for **4**), and 416.0 nm (used for **5**) were produced from the harmonics or their hydrogen Raman-shifted laser lines of the Nd:YAG lasers that were used in the ns-TR^3 experiments. The pump pulse excited the sample to initiate the photochemical reactions, and the probe pulse interrogated the sample and the intermediate species produced by the pump pulse. The laser beams were lightly focused and overlapped onto a flowing liquid stream of sample. A pulse delay generator was employed to electronically control the time delay between the pump and probe laser beams from the two different Nd:YAG lasers operated at a repetition rate of 10 Hz. The Raman scattered light was acquired using a backscattering geometry and detected by a liquid nitrogen-cooled CCD detector. The ns-TR^3 spectra presented in this paper were obtained from subtraction of an appropriately scaled probe-before-pump spectrum from the corresponding pump−probe resonance Raman spectrum to remove nontransient bands. The Raman bands of MeCN were employed to calibrate the Raman shifts of the Raman spectra with an estimated accuracy of 5 cm^{-1}. The sample concentrations in ns-TR^3 were ~5 × 10^{-4} M.[14]

Computational Details. All of the calculations here were performed with the Gaussian 09 software package.[15] DFT was employed using the M062X hybrid functional, which was found to validate the prediction of relative stability of radical species by several other groups.[10,16] Geometry optimizations, harmonic vibrational frequency calculations, gas Gibbs free energy, intrinsic reaction coordinate (IRC) calculations, spin-density analyses, Raman activity spectra, and UV−vis spectra were carried out with the 6-311+G** basis set for all atoms. All stationary points were optimized without point group symmetry. Analytical second derivative computations were performed for all stationary points to confirm the optimized structures as either minima or first-order saddle points. IRC[17] calculations were performed to confirm that the transition states connected the relevant reactants and products. To evaluate the effect of solvent polarity on the relative stability of np and pp, single-point energy calculations were performed with the integral equation formalism polarizable continuum model (IEFPCM) in cyclohexane (ε = 2.0165), ACN (ε = 35.688), and H_2O (ε = 78.3553) on the gas-phase geometries. The radii and nonelectrostatic terms were taken from Truhlar and co-workers' universal solvation model (SMD).[18] Solvation single-point computations utilized the 6-311++G** basis set for all atoms. The discussion is based on solvated Gibbs free energy G_{solv}, which was estimated as G_{solv}= E_{solv} (SMD-calculated) + ΔG_{corr_gas}, where E_{solv} (SMD-calculated) refers to the solvation single point energy and ΔG_{corr_gas} refers to the thermal correction to the free energy of the solute in the gas phase.[19]

ASSOCIATED CONTENT

Supporting Information

The Supporting Information is available free of charge on the ACS Publications website at DOI: 10.1021/acs.joc.6b00620.

Table 1S and Figures 1S−5S of selected computational results discussed in the text, including Cartesian coordinates and energies for all calculated structures found in this work (PDF)

AUTHOR INFORMATION

Corresponding Authors

*E-mail: anini1984@163.com.

*E-mail: phillips@hku.hk.

Notes

The authors declare no competing financial interest.

ACKNOWLEDGMENTS

The research was sponsored in part by a grants from the Research Grants Council of Hong Kong (HKU 17301815) to D.L.P. and the National Science Fund of China (21503167) and Shaanxi Province Science Fund (2016JQ2009) to J.M. and partial support from the Areas of Excellence Scheme (Grant AoE/P-03/08) and the UGC Special Equipment Grant (SEG-HKU-07). We thank Professor Peter Wan and Dr. Yunyan Hou at the University of Victoria for generously providing the samples of 2-(1-hydroxyethyl)-9,10-anthraquinone (**3**) and 2-(p-hydroxy-methyl)-phenylanthraquinone (**4**) used in this study.

REFERENCES

(1) Guay, D. R. P. *Ann. Pharmacother.* **1999**, *33*, 1083.

(2) Miranda, M. A.; Castell, J. V.; Hernandez, D.; Gomez-Lechon, M. J.; Bosca, F.; Morera, I. M.; Sarabia, Z. *Chem. Res. Toxicol.* **1998**, *11*, 172.

(3) (a) Furuta, T.; Torigai, H.; Sugimoto, M.; Iwamura, M. *J. Org. Chem.* **1995**, *60*, 3953. (b) Furuta, T.; Hirayama, Y.; Iwamura, M. *Org. Lett.* **2001**, *3*, 1809. (c) Brinson, R. G.; Jones, P. B. *Org. Lett.* **2004**, *6*, 3767. (d) Brinson, R. G.; Hubbard, S. C.; Zuidema, D. R.; Jones, P. B. J. *J. Photochem. Photobiol., A* **2005**, *175*, 118. (e) Jones, P. B.; Brinson, R. G.; Sarma, S. J.; Elkazaz, S. *Org. Biomol. Chem.* **2008**, *6*, 4203.

DOI: 10.1021/acs.joc.6b00620
J. Org. Chem. 2016, 81, 5330−5336

(f) Ren, M.-G.; Bi, N.-M.; Mao, M.; Song, Q.-H. J. *J. Photochem. Photobiol., A* **2009**, *204*, 13. (g) Sarma, S. J.; Jones, P. B. *J. Org. Chem.* **2010**, *75*, 3806.
(4) (a) Ledger, M. B.; Porter, G. *J. Chem. Soc., Faraday Trans. 1* **1972**, *68*, 539. (b) Bensasson, R. V.; Gramain, J. C. *J. Chem. Soc., Faraday Trans. 1* **1980**, *76*, 1801. (c) Knoll, M.; Weidemann, F.; Hennig, H. *React. Kinet. Catal. Lett.* **1988**, *36*, 411. (d) Leigh, W. J.; Lathioor, E. C., St; St. Pierre, M. J. *J. Am. Chem. Soc.* **1996**, *118*, 12339. (e) Du, Y.; Xue, J. D.; Li, M. D.; Phillips, D. L. *J. Phys. Chem. A* **2009**, *113*, 3344. (f) Chuang, Y. P.; Xue, J. D.; Du, Y.; Li, M. D.; An, H. Y.; Phillips, D. L. *J. Phys. Chem. B* **2009**, *113*, 10530. (g) Li, M. D.; Du, Y.; Chuang, Y. P.; Xue, J. D.; Phillips, D. L. *Phys. Chem. Chem. Phys.* **2010**, *12*, 4800. (h) Li, M. D.; Huang, J.; Liu, M.; Li, S.; Ma, J.; Phillips, D. L. *J. Phys. Chem. B* **2015**, *119*, 2241.
(5) (a) Walling, C.; Gibian, M. *J. Am. Chem. Soc.* **1965**, *87*, 3361. (b) Wagner, P. J.; Truman, R. J.; Scaiano, J. C. *J. Am. Chem. Soc.* **1985**, *107*, 7093. (c) Wagner, P. J.; Kemppainen, A. E.; Schott, H. N. *J. Am. Chem. Soc.* **1973**, *95*, 5604. (d) Wagner, P. J.; Park, B.-S. *Org. Photochem.* **1991**, *11*, 227. (e) Ramseier, M.; Senn, P.; Wirz, J. *J. Phys. Chem. A* **2003**, *107*, 3305. (f) Nicodem, D. E.; Silva, R. S.; Togashi, D. M.; da Cunha, M. F. V. *J. Photochem. Photobiol., A* **2005**, *175*, 154. (g) Du, Y.; Xue, J. D.; Li, M. D.; Phillips, D. L. *J. Phys. Chem. A* **2009**, *113*, 3344.
(6) (a) Schwarz, H. A. *J. Chem. Educ.* **1981**, *58*, 101. (b) Lhiaubet, V.; Paillous, N.; Chouini-Lalanne, N. *Photochem. Photobiol.* **2001**, *74*, 670.
(7) (a) Wagner, P. J.; Kemppainen, A. E.; Schott, H. N. *J. Am. Chem. Soc.* **1973**, *95*, 5604. (b) Boscá, F.; Cosa, G.; Miranda, M. A.; Scaiano, J. C. *Photochem. Photobiol. Sci.* **2002**, *1*, 704. (c) Jornet, D.; Bartovsky, P.; Domingo, L. R.; Tormos, R.; Miranda, M. A. *J. Phys. Chem. B* **2010**, *114*, 11920. (d) Jornet, D.; Tormos, R.; Miranda, M. A. *J. Phys. Chem. B* **2011**, *115*, 10768.
(8) (a) Xu, Y.; Chen, X.; Fang, W.-H.; Phillips, D. L. *Org. Lett.* **2011**, *13*, 5472. (b) Chen, X.; Zhang, Q.; Xu, Y.; Fang, W.; Phillips, D. L. *J. Org. Chem.* **2013**, *78*, 5677. (c) Dai, J.; Han, J.; Chen, X.; Fang, W.; Ma, J.; Phillips, D. L. *Phys. Chem. Chem. Phys.* **2015**, *17*, 27001.
(9) Ding, L.; Shen, L.; Chen, X.-B.; Fang, W.-H. *J. Org. Chem.* **2009**, *74*, 8956.
(10) Zhao, Y.; Schultz, N. E.; Truhlar, D. G. *J. Chem. Theory Comput.* **2006**, *2*, 364.
(11) Ermolaev, V. L.; Terenin, A. N. *J. Chim. Phys.* **1958**, *55*, 698.
(12) (a) Weinberg, D. R.; Gagliardi, C. J.; Hull, J. F.; Murphy, C. F.; Kent, C. A.; Westlake, B. C.; Paul, A.; Ess, D. H.; McCafferty, D. G.; Meyer, T. J. *Chem. Rev.* **2012**, *112*, 4016. (b) Harshan, A. K.; Yu, T.; Soudackov, A. V.; Hammes-Schiffer, S. *J. Am. Chem. Soc.* **2015**, *137*, 13545.
(13) (a) Hou, Y. Y.; Wan, P. *Photochem. Photobiol. Sci.* **2008**, *7*, 588. (b) Hou, Y. Y.; Huck, L. A.; Wan, P. *Photochem. Photobiol. Sci.* **2009**, *8*, 1408. (c) Ma, J.; Su, T.; Li, M.-D.; Du, W.; Huang, J.-Q.; Guan, X. G.; Phillips, D. L. *J. Am. Chem. Soc.* **2012**, *134*, 14858−14868.
(14) Ma, C.; Kwok, W. M.; Chan, W. S.; Du, Y.; Kan, J. T. W.; Toy, P. H.; Phillips, D. L. *J. Am. Chem. Soc.* **2006**, *128*, 2558.
(15) Frisch, M. J.; Trucks, G. W.; Schlegel, H. B.; Scuseria, G. E.; Robb, M. A.; Cheeseman, J. R.; Scalmani, G.; Barone, V.; Mennucci, B.; Petersson, G. A.; Nakatsuji, H.; Caricato, M.; Li, X.; Hratchian, H. P.; Izmaylov, A. F.; Bloino, J.; Zheng, G.; Sonnenberg, J. L.; Hada, M.; Ehara, M.; Toyota, K.; Fukuda, R.; Hasegawa, J.; Ishida, M.; Nakajima, T.; Honda, Y.; Kitao, O.; Nakai, H.; Vreven, T.; Montgomery, J. A., Jr.; Peralta, J. E.; Ogliaro, F.; Bearpark, M.; Heyd, J. J.; Brothers, E.; Kudin, K. N.; Staroverov, V. N.; Kobayashi, R.; Normand, J.; Raghavachari, K.; Rendell, A.; Burant, J. C.; Iyengar, S. S.; Tomasi, J.; Cossi, M.; Rega, N.; Millam, J. M.; Klene, M.; Knox, J. E.; Cross, J. B.; Bakken, V.; Adamo, C.; Jaramillo, J.; Gomperts, R.; Stratmann, R. E.; Yazyev, O.; Austin, A. J.; Cammi, R.; Pomelli, C.; Ochterski, J. W.; Martin, R. L.; Morokuma, K.; Zakrzewski, V. G.; Voth, G. A.; Salvador, P.; Dannenberg, J. J.; Dapprich, S.; Daniels, A. D.; Farkas, O.; Foresman, J. B.; Ortiz, J. V.; Cioslowski, J.; Fox, D. J. *Gaussian 09*; Gaussian, Inc.: Wallingford, CT, 2009.
(16) (a) Krishnan, R.; Binkley, J. S.; Seeger, R.; Pople, J. A. *J. Chem. Phys.* **1980**, *72*, 650. (b) Clark, T.; Chandrasekhar, J.; Spitznagel, G. W.; Schleyer, P. V. *J. Comput. Chem.* **1983**, *4*, 294.
(17) Foresman, J. B.; Keith, T. A.; Wiberg, K. B.; Snoonian, J.; Frisch, M. J. *J. Phys. Chem.* **1996**, *100*, 16098.
(18) Marenich, A. V.; Cramer, C. J.; Truhlar, D. G. *J. Phys. Chem. B* **2009**, *113*, 6378.
(19) (a) Ho, J.; Klamt, A.; Coote, M. L. *J. Phys. Chem. A* **2010**, *114*, 13442. (b) Guo, Z.; Guan, X.; Huang, J.-S.; Tsui, W.-M.; Lin, Z.; Che, C.-M. *Chem. - Eur. J.* **2013**, *19*, 11320. (c) Harvey, M. E.; Musaev, D. G.; Du Bois, J. *J. Am. Chem. Soc.* **2011**, *133*, 17207.

DOI: 10.1021/acs.joc.6b00620
J. Org. Chem. 2016, 81, 5330−5336